3-2013

An in Situ Experimental Study of Grain Growth in a Nanocrystalline Fe91Ni8Zr1 Alloy

Hasan Kotan
North Carolina State University

Kris A. Darling
U.S. Army Research Laboratory, Weapons and Materials Research Directorate, RDRL-WMM-F, Aberdeen Proving Ground

Mostafa Saber
Portland State University, msaber@pdx.edu

Ronald O. Scattergood
North Carolina State University

Carl C. Koch
North Carolina State University

Citation Details

Kotan, H., Darling, K. A., Saber, M., Scattergood, R. O., & Koch, C. C. (2013). An in situ experimental study of grain growth in a nanocrystalline Fe91Ni8Zr1 alloy. Journal of Materials Science, 48(5), 2251-2257.

J Mater Sci (2013) 48:2251–2257
DOI 10.1007/s10853-012-7002-1

An in situ experimental study of grain growth in a nanocrystalline $Fe_{91}Ni_8Zr_1$ alloy

Hasan Kotan · Kris A. Darling · Mostafa Saber · Ronald O. Scattergood · Carl C. Koch

Received: 20 August 2012 / Accepted: 30 October 2012 / Published online: 27 November 2012

Abstract Grain growth and microstructural evolution of thermally stabilized $Fe_{91}Ni_8Zr_1$ were investigated by in situ and ex situ studies. Our investigations suggest that the microstructural evolution is fairly slow and the microstructure shows stabilization up to about 700 °C. Above this temperature, a certain fraction of grains grow abnormally into the nanocrystalline matrix, resulting in a bimodal microstructure and causing the complete loss of thermal stability. The reason for abnormal grain growth and the loss of thermal stability is identified as the appearance of the fcc γ-phase and consequent reduction in the total area of grain boundaries and the overall stored energy.

List of symbols

M	Grain boundary mobility
Q	Activation energy
v	Velocity of grain boundary
D	Grain diameter
h	Specimen thickness
δD	Incremental growth
δG	Change in volume free energy
$\delta\Gamma_s$	Change in surface energy
$\delta\Gamma_{i/gb}$	Change in the interphase energy-grain boundary energy
A_s	Free surface area
A_i	Grain interface area
V	Volume of grains
g	Bulk free energy per volume
Γ_s	Surface energy per area
Γ_i	α-to-γ interface energy per area
Γ_{gb}	Grain boundary energy per area
P	Pressure acting on the grain interfaces
$\tilde{D}$	Diffusivity
D_o	Frequency factor
r	Diffusion distance
t	Annealing time
T	Annealing temperature
R	Gas constant

H. Kotan (✉) · M. Saber · R. O. Scattergood · C. C. Koch
Department of Materials Science and Engineering, NC State University, 911 Partners Way, Room 3002, Raleigh, NC 27695-7907, USA
e-mail: hkotan@ncsu.edu

K. A. Darling
U.S. Army Research Laboratory, Weapons and Materials Research Directorate, RDRL-WMM-F, Aberdeen Proving Ground, Aberdeen, MD 21005-5069, USA

Introduction

Nanostructured materials are promising for structural applications [1]. However, their widespread application is limited by an inherently high driving force for thermally induced grain growth, even at low temperatures [2–4]. Accordingly, the understanding of and control over grain growth in nanoscale materials is of great technological and scientific importance [5] as many physical properties (i.e., mechanical properties) are functions of the average grain size and the grain size distribution within the microstructure [6, 7].

In the last decade, extensive investigations into the stabilization of metallic nanocrystalline microstructures have been carried out to improve their stability. In spite of a high driving force for grain growth, significant stabilization has been reported [8–13]. This stabilization and resistance to grain growth has been attributed to reducing

the energy of the grain boundaries with solute segregation (i.e., thermodynamic stabilization) [14] or reducing the mobility of the grain boundaries by grain boundary pinning (kinetic stabilization) [15]. Nevertheless, the reported works have, for the majority, been based on analysis of evolved microstructures post thermal processing, and not by direct observation at temperature. This is of fundamental importance as it is unclear how grain coarsening occurs in systems stabilized against growth. The advantage of in situ microstructural evolution studies comes from directly observing this phenomenon and its kinetics such that the respective mechanism and driving force can be understood in detail.

In this work, we used in situ transmission electron microscopy (TEM) with video imaging and in situ X-ray diffractometry (XRD) to directly follow grain growth and microstructural evolution in such a system as a function of temperature. Ex situ experiments are also reported giving a broader perspective of the microstructure at longer annealing times. The information obtained from these experiments enables the real time observation of microstructural evolution and phase transformation and provides a unique view of dynamic reactions as they occur.

Experiments

A ternary $Fe_{91}Ni_8Zr_1$ alloy was chosen as the stabilized Fe-based nanocrystalline alloy for this study. As starting materials, appropriate masses of elemental Fe (99.9 %), Ni (99.9 %), and Zr (99.7 %) powders were mixed with 440C stainless steel balls and sealed in a hardened steel vial under an argon atmosphere ($O_2 < 2$ ppm) before milling. Ball milling was performed using a SPEX 8000 model mixer-mill for 20 h. After milling, powders were isochronally annealed at 600, 700, 800, and 900 °C in a 98 % Ar + 2 % H_2 gas atmosphere for 1 h with subsequent cooling in the furnace where the cooling rate was less than 2–3 °C per second. The as-milled powder was used as the starting material for annealing at each temperature. Microstructure of the samples is characterized by focused ion beam channeling contrast imaging (FIB-CCI). FIB-CCI images were obtained using backscattered electrons produced by the ion beam from one powder particle.

The ion beam was also used to prepare an electron transparent sample from the as-milled powder for the in situ transmission electron microscopy (TEM) annealing experiments. The sample was mounted in the Aduro holder [16] and imaged in a Hitachi HF-2000 TEM. The Aduro system uses a flat, ceramic membrane as the active specimen support to enable fast, stable, and accurate thermal analysis. The membrane has a small thermal mass which allows for extremely fast heating rates up to 10^6 °C/s with virtually instantaneous temperature stabilization and accuracy of ±0.5–3 °C. The whole experiment was recorded with a video imaging in bright field (BF) mode to directly observe grain growth in the initially nanocrystalline sample. The increment of the temperature was 50 °C during in situ annealing.

High temperature XRD analysis was carried out using an Anton Paar HTK 2000. Samples consisted of a thin layer of powder place onto a Pt strip. A given sample was then brought into alignment on the optical axis of the diffractometer. The heating chamber was pumped down, under a vacuum of approximately 10^{-3} Torr and backfilled with a He 3 % hydrogen forming gas to prevent oxidation of the powders during examination. The sample was then resistively heated to temperature at a rate of 60 °C/min, at which point it endured a 10 min isothermal anneal, before performing a 17 min long diffraction scan at the respective temperature. The sample temperature was increased to the next desired set point and the isothermal/scanning process repeated as done previously. This process was repeated to cover the following temperature range of 30, 500, 600, 700, 750, 800, 900, and again at 31 °C to complete the test. The grain size at temperature was calculated by the Scherrer method.

Results and discussion

Figure 1 illustrates the morphological evolution of nanocrystalline $Fe_{91}Ni_8Zr_1$ subjected to the in situ thermal annealing in the TEM up to 900 °C. The snapshots were taken from the video and, in general, the majority of the observed grain growth ceased within the time frame given in Fig. 1. The real time monitoring of the microstructure during in situ thermal treatments revealed negligible grain growth until 500 °C. Grain growth became discernible at 500 °C and all visible grains in the view remained smaller than 50 nm up to annealing to 600 °C. Gradual increase of the average grain size (i.e., average grain diameter) is observed with the increase in temperature and a few grains reached the size of 100 nm after 15 s at 700 °C. Above this temperature, a certain fraction of grains grew rapidly into the nanocrystalline matrix within the first few seconds of annealing, resulting in a bimodal microstructure at 750 °C. Abnormal grain growth continued at the expense of their neighbors with the increase in temperature to 800 and 850 °C. Further increase in annealing temperature to 900 °C caused the complete consumption of the smaller grains in the microstructure and led to normal grain growth where the microstructure exhibits a uniform increase in size. The last micrograph in Fig. 1 shows that grains in the viewing area are fairly uniform and reached the size of

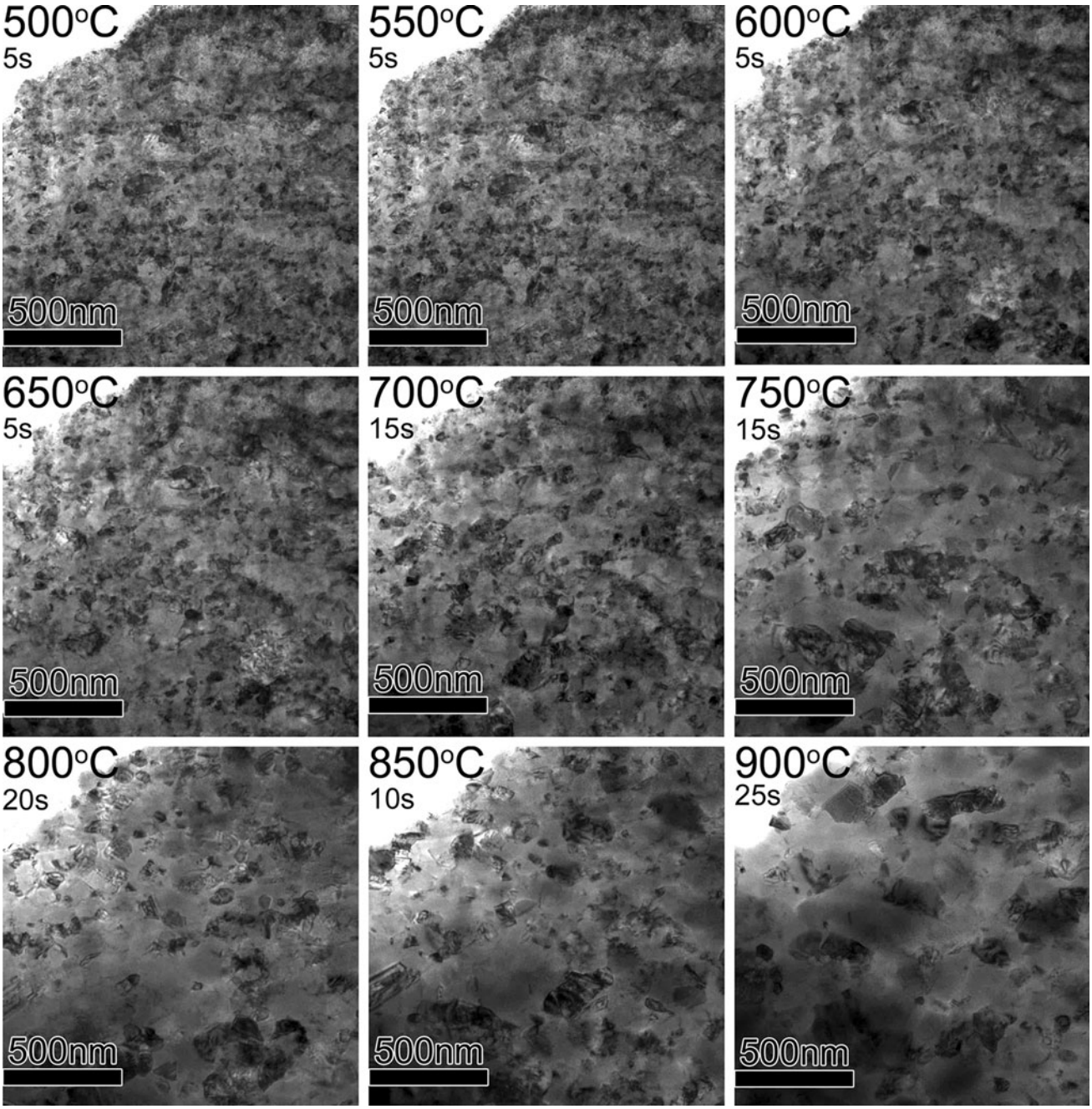

Fig. 1 Sequence of plan-view bright field TEM micrographs showing the morphological evolution of nanocrystalline $Fe_{91}Ni_8Zr_1$ alloy during in situ thermal treatments. Below 700 °C, the nanocrystalline microstructure remains stable. Above this temperature, a sudden abnormal grain growth is observed resulting in loss of thermal stability. All images are recorded at the same magnification. Temperature and the time at given temperature are displayed at the *upper left corner* of each micrograph

400 nm after 25 s at 900 °C, and the nanocrystalline microstructure is lost.

In addition to rapid and abnormal grain growth above 700 °C, we also observed a loss of contrast between neighboring grains with the eventual disappearance of the grains or the boundary between them. The orientation of two grains has to be within a few degrees to appear in the same image. The fact that neighboring regions appear/disappear suggests that these regions represent grains that have rotated into alignment with their neighbors to attain the orientation of one of its neighbors. The driving force for the grain rotation might arise from the tendency of the grains to reduce their overall grain boundary energy due to misorientations. This rotation of the adjoining grains is

presumably required for crystallographic alignment before the subsequent merging of the two grains to attain the minimum crystallographic energy state [17].

In situ TEM observation indicated that microstructural changes and grain growth are fairly slow as the nanocrystalline state remains stable until 700 °C. However, they become extremely fast especially for the first few seconds of annealing at above 750 °C, resulting in sudden abnormal grain growth and loss of thermal stability. The view of the microstructure was limited in the in situ TEM experiment and the annealing time was rather short. We took advantage of ex situ annealing to investigate the microstructure subjected to longer annealing time and to eliminate the possible influences to grain growth by the free surfaces of the TEM sample. Figure 2 reveals low magnification FIB images of the as-milled specimen and annealed at 600, 700, 800, and 900 °C for 1 h. Upon comparison of the as-milled microstructure with samples annealed isochronally, we see that there is not a significant grain growth after 1 h annealing at 600 °C. Above this temperature, at 700 °C, a certain fraction of grains grow abnormally into the nanocrystalline matrix, resulting in a bimodal microstructure. That is, a few grains grew to above the nanoscale, greater than 100 nm, while the majority of the microstructure remained nanoscale. The extent of abnormal grain growth continues to increase at 800 °C, consuming the majority of the microstructure and leaving only a very small fraction of the microstructure nanocrystalline. Further increases in annealing temperature to 900 °C caused the complete consumption of the smaller grains (nano and ultrafine) in $Fe_{91}Ni_8Zr_1$, which leads to the formation of a more uniform large grain assembly.

Consistent observation from ex situ FIB and in situ TEM results demonstrates that the majority of the nanocrystalline microstructure of the ternary alloy remains stable up to about 700 °C showing excellent thermal stabilization compared to reported examples of pure iron and Fe–Ni alloys [18–21]. It is postulated that the grain growth in Fe–Ni–Zr alloy below 700 °C was blocked by the interaction between the grain boundaries and zirconium solute by the solute drag affect and reduction in the grain boundary energy [22]. Above 700 °C, the development of abnormal grain growth and consequent loss of thermal stability was observed by the in situ and ex situ studies. Dake and Krill [23] reported that the abnormal grain growth in binary Fe–Ti alloy is due to the α-to-γ transformation above 900 °C. This phenomenon and its impact on microstructure evolution and abnormal grain growth were investigated by in situ X-ray diffractometry for identification of the phases present during thermal annealing.

Figure 3 shows diffraction patterns obtained for $Fe_{91}Ni_8Zr_1$ during isochoric annealing up to 900 °C for a total duration of 4 h, such that analysis at each temperature took approximately 30 min. A slight horizontal shift as a function of temperature was noticed in the peak positions due to thermal expansion of the lattice with increase in temperature [24]. The XRD results reveal that the microstructure remains pure bcc up to annealing to 650 °C where an fcc peak was first observed. The intensity of the fcc peak at 650 °C is substantially lower suggesting that the volume fraction of the fcc phase is very small and it is just beginning to nucleate and grow. It is worth noting that the fcc peak is much narrower than the bcc peak at and above 700 °C. While the bcc peak narrows with temperature, it remains fairly wide even at 800–900 °C. It indicates that even at small volume fractions the fcc grains are much larger on average than the bcc grains, implying that the large grains formed above 700 °C are fcc, while small grains detected in the microstructure are still bcc. Comparison of Figs. 1 and 2 with the data obtained from Fig. 3 suggests that the bcc to fcc phase transformation is, indeed, responsible for the rapid formation of large (fcc) grains in (bcc) nanocrystalline matrix above 700 °C and caused the loss of thermal stability. To evaluate this effect, we can estimate the driving pressure P for grain growth, which determines the velocity v.

$$v = M \cdot P = M_o e^{-Q/RT} \cdot P \tag{1}$$

M is the grain boundary mobility and Q is the activation energy. If we assume that the grains in the nanocrystalline TEM specimen (Fig. 1) are hexagonal prisms (as in thin films) of width D and thickness h, and define the driving force for grain boundary migration as the total free energy reduction for incremental growth δD, then the driving force for an fcc γ-Fe grain growing in a surrounding bcc α-Fe grain matrix is due to the change in volume free energy (δG), surface energy ($\delta \Gamma_s$), and interphase energy-grain boundary energy ($\delta \Gamma_{\mathrm{i/gb}}$).

$$\delta G = (g^{\gamma} - g^{\alpha})\delta V = (g^{\gamma} - g^{\alpha})\frac{3\sqrt{3}}{2} Dh\delta \mathrm{D} \tag{2}$$

$$\delta \Gamma_s = \left(\Gamma_s^{\gamma} - \Gamma_s^{\alpha}\right)\delta A_s = \left(\Gamma_s^{\gamma} - \Gamma_s^{\alpha}\right)\frac{3\sqrt{3}}{2} D\delta \mathrm{D} \tag{3}$$

$$\delta \Gamma_{\mathrm{i/gb}} = \left(\Gamma_i^{\gamma\alpha}\delta A_{\mathrm{i}} - 3h\Gamma_{\mathrm{gb}}^{\alpha}\delta \mathrm{D}\right) = \left(\Gamma_i^{\gamma\alpha} - \Gamma_{\mathrm{gb}}^{\alpha}\right)3h\delta \mathrm{D} \tag{4}$$

A_s is the free surface area, A_{i} is the grain interface area, V is the volume of grains, g is the bulk free energy per volume, Γ_s is the surface energy per area, Γ_{i} is the α-to-γ interface energy per area, and Γ_{gb} is the grain boundary energy per area. The pressure acting on the grain interfaces will be

$$P = -\frac{1}{A_{\mathrm{i}}}\left[\frac{\delta G}{\delta D} + \frac{\delta \Gamma_s}{\delta D} + \frac{\delta \Gamma_{\mathrm{i/gb}}}{\delta D}\right] \tag{5}$$

Combination of Eq. (2–5) will give Eq. (6) where $P > 0$ will be outward and will drive grain growth.

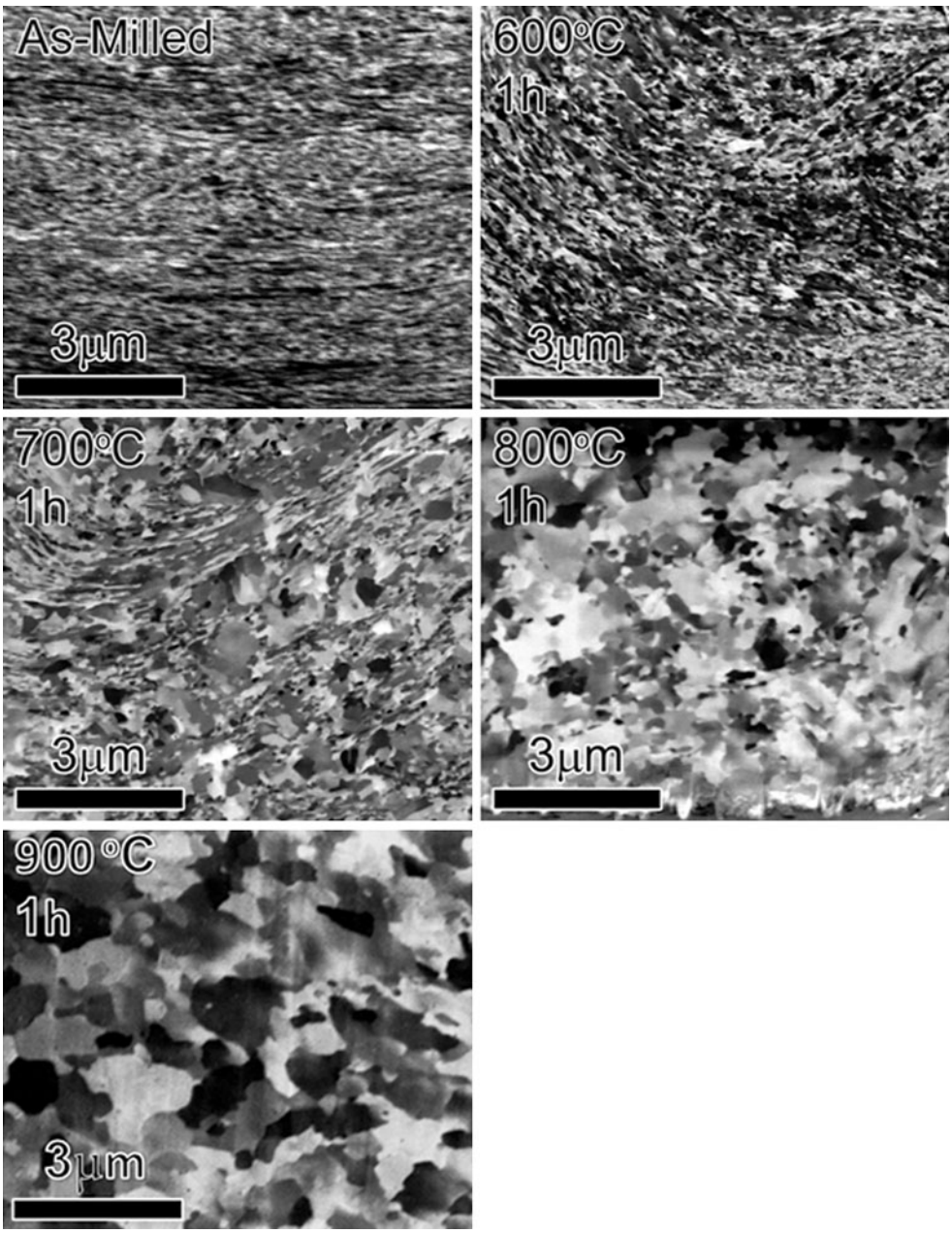

Fig. 2 Channeling contrast images of $Fe_{91}Ni_8Zr_1$ as-milled, annealed at 600, 700, 800, and 900 °C. There is no significant grain growth after 1 h annealing at 600 °C. Above 700 °C, a certain fraction of grains grow abnormally, the nanocrystalline state is lost and sudden grain growth is observed

$$P = -\left[\frac{1}{3Dh}\right]\left[\frac{3\sqrt{3}}{2}Dh(g^{\gamma} - g^{\alpha}) + \frac{3\sqrt{3}}{2}D\left(\Gamma_s^{\gamma} - \Gamma_s^{\alpha}\right) + 3h\left(\Gamma_{\mathrm{i}}^{\gamma\alpha} - \Gamma_{\mathrm{gb}}^{\alpha}\right)\right] \quad (6)$$

$$P = -\left[\frac{\sqrt{3}}{2}(g^{\gamma} - g^{\alpha}) + \frac{\sqrt{3}}{2h}\left(\Gamma_s^{\gamma} - \Gamma_s^{\alpha}\right) + \frac{1}{D}\left(\Gamma_{\mathrm{i}}^{\gamma\alpha} - \Gamma_{\mathrm{gb}}^{\alpha}\right)\right] \quad (7)$$

The grain boundary energy, interphase boundary energy, α-to-γ volume free energy change, and α-to-γ surface energy change are reported to be 0.70 J/m^2 [25], 0.8 J/m^2 [26], 1230 J/mol at 727 °C [27], and 0.053 J/m^2 [26], respectively. If $\gamma = \alpha$ (before phase transformation), then the driving pressure $P = 0$. If γ grain forms in α matrix, it will change the pressure on grain boundaries and there will be a driving force to grow the γ grains in the α-grain surroundings. If we use 150 nm as the film thickness, the pressure for grain growth $P = +150$ MPa. By comparison of in situ TEM and ex situ FIB images, it appears that surface energy in the in situ TEM sample does not affect the abnormal grain growth significantly. Moreover, the

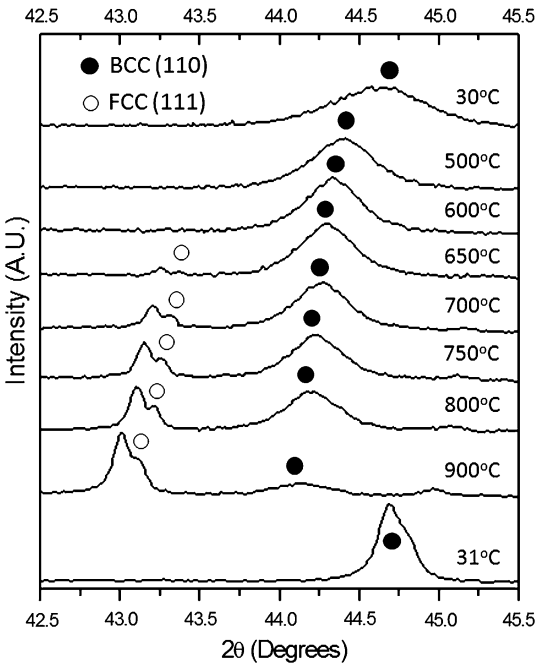

Fig. 3 In situ XRD scans of a $Fe_{91}Ni_8Zr_1$ alloy during isochoric annealing from room temperature to 900 °C. The first scan 30 °C is the initial microstructure showing broad bcc Fe peak. As indicated, fcc Fe peak appears around 650 °C and bcc Fe peak remains stable up to 900 °C. The last scan 31 °C is after heat treatment showing the disappearance of the fcc Fe peaks and the reappearance of the bcc Fe

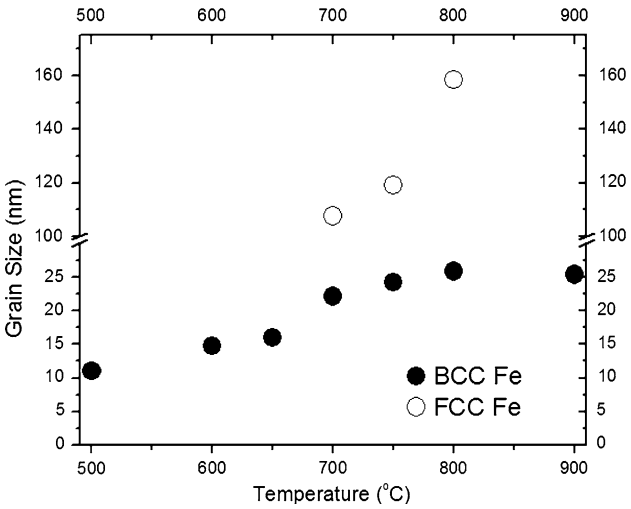

Fig. 4 Grain size analysis of the diffraction peaks shown in Fig. 3, plotted against annealing temperature for the duration of 30 min at each temperature. The bcc phase consists of nanoscale grains until 900 °C, which grow an initial size of 10 nm to a final size of 25 nm. The fcc peak was intense enough to calculate grain size at 700 °C

calculations for P indicate that crucial contributions to grain growth come from the reduction in the grain boundary energy and, mostly, from the volume free energy change for α-to-γ. This change is large (1230 J/mol) which gives the γ grains a significant growth advantage over α grains, thereby triggering sudden grain growth in abnormal manner and eventually causing loss of thermal stability. The last XRD scan at 31 °C is after heat treatment and shows the disappearance of the fcc γ peaks and the reappearance of the bcc α peaks.

The bcc phase remains up to 900 °C (see Fig. 3) even though it is expected to vanish according to the Fe–Ni–Zr phase diagram [28]. It is well-known that the austenite phase nucleates at GBs, triple points or near regions in Fe-based alloys [29], and the alloying elements, such as nickel, are redistributed during the nucleation and growth of the austenite phase [30] enriching the solute atoms at some regions and depleting it in others. We propose that the initial solute distribution of Ni (an fcc stabilizer), locally high in some regions, will favor the nucleation and growth of austenite at temperatures near the bcc to fcc transition (∼700 °C). The growth and formation of these new fcc grains as temperature increases >700 °C will lead to the incorporation of Ni in higher concentrations than the average global content within or near the fcc grains. Through mass balance, the amount of nickel consumed or redistributed during austenite formation and growth must also be removed or redistributed from the surrounding matrix of nanograins. The resistance to transformation by these newly depleted (lower nickel content) nanograined regions is now a function of both composition and temperature as prescribed by the α-to-γ equilibrium phase limits. As more austenite grains nucleate and grow, the local nickel solute content in some regions may approach zero, thereby pushing the transition temperature up to that of pure iron, 913 °C, locally. The diffusivity (for Fe—10 at % Ni) and diffusion distance calculated from Eqs. (8) and (9) were found to be 2.72×10^{-14} cm^2/s (based on Q and D_o values obtained from Ref. [31]) and 70 nm, respectively, after 30 min annealing at 900 °C.

$$\tilde{D} = D_o \exp(-Q/RT) \tag{8}$$

$$r = \sqrt{\tilde{D}t} \tag{9}$$

$\tilde{D}$ is the diffusivity, D_o is the frequency factor, Q is the activation energy, r is the diffusion distance, t is the annealing time, T is the annealing temperature, and R is the gas constant. This suggests that nickel atoms had the opportunity during thermal annealing to be redistributed over length scales approximately equal to or larger than the grain size within the retained nanocrystalline regions. This implies that the small grains observed at 800–and 900 °C in the FIB images in Fig. 2 are bcc α grains which never transformed to or were consumed by fcc γ grains during thermal annealing.

Figure 4 shows the Scherrer grain size analysis of the diffraction peaks reported in Fig. 3. It reveals that the grains of the bcc phase grow from an initial size of 10 nm

to a final size of 25 nm after 30 min annealing at 900 °C (for a total duration of 4 h). The fcc phase appears at 650 °C, but the corresponding diffraction peak is not intense enough to allow calculation of the grain size. The estimated grain size of the fcc phase was approximately 105 nm at 700 °C, and proceeded to increase with increasing annealing temperature.

Conclusions

The observations from in situ and ex situ experiments reported above and the information obtained from these studies enable us to understand the grain growth in stabilized Fe–Ni-based alloys. From our observations, it is suggested that the microstructural evolution is fairly slow and the microstructure shows a solid stabilization up to about 700 °C. This is attributed to zirconium segregation to grain boundaries and the solute drag effect. Above 700 °C, the grain growth kinetics becomes extremely fast, especially for the first few seconds of annealing and causes a sudden grain growth in abnormal manner. The reasons for abnormal grain growth and the loss of thermal stability were identified as the appearance of the fcc γ phase and consequent reduction in the total area of grain boundaries and the overall stored energy in the sample.

Acknowledgements The research reported in this paper was supported by NSF-DMR under grant number 1005677.

References

1. Gleiter H (1989) Prog Mater Sci 33(4):223
2. Birringer R (1989) Mater Sci Eng A 117:33
3. Suryanarayana C (2002) Jom-J Min Metals Mater Soc 54(9):24
4. Koch CC, Scattergood RO, Darling KA, Semones JE (2008) J Mater Sci 43(23–24):7264
5. Koch CC (2007) J Mater Sci 42(5):1403
6. Suryanarayana C (1995) Int Mater Rev 40(2):41
7. Gleiter H (1992) Adv Mater 4(7–8):474
8. VanLeeuwen BK, Darling KA, Koch CC, Scattergood RO, Butler BG (2010) Acta Mater 58(12):4292
9. Krill CE, Ehrhardt H, Birringer R (2005) Zeitschrift Fur Metallkunde 96(10):1134
10. Shaw L, Luo H, Villegas J, Miracle D (2003) Acta Mater 51(9):2647
11. Frolov T, Darling KA, Kecskes LJ, Mishin Y (2012) Acta Mater 60(5):2158
12. Darling KA, VanLeeuwen BK, Koch CC, Scattergood RO (2010) Mater Sci Eng, A 527(15):3572
13. Perez RJ, Jiang HG, Dogan CP, Lavernia EJ (1998) Metall Mater Transac A 29(10):2469
14. Kirchheim R (2007) Acta Mater 55(15):5129
15. Michels A, Krill CE, Ehrhardt H, Birringer R, Wu DT (1999) Acta Mater 47(7):2143
16. www.protochips.com
17. Smith CJE, Dillamore IL (1970) Metal Sci 4(1):161
18. Kotan H, Saber M, Koch CC, Scattergood RO (2012) Mater Sci Eng, A 552:310
19. Darling KA, VanLeeuwen BK, Semones JE, Koch CC, Scattergood RO, Kecskes LJ, Mathaudhu SN (2011) Mater Sci Eng, A 528(13–14):4365
20. Shen TD, Schwarz RB, Feng S, Swadener JG, Huang JY, Tang M, Zhang H, Vogel SC, Zhao YS (2007) Acta Mater 55(15):5007
21. Malow TR, Koch CC (1997) Acta Mater 45(5):2177
22. Kotan H, Darling KA, Saber M, Koch CC, Scattergood RO (2012) J Alloys Comp. doi:10.1016/j.jallcom.2012.10.179
23. Dake JM, Krill CE (2012) Scripta Mater 66(6):390
24. Culity BD (1977) Element of X-ray diffraction, 2nd edn. Addison-Wesley, MA
25. Murr LE (1975) Interfacial phenomena in metals and alloys. Addision-Wesley, MA
26. Yang Z, Johnson RA (1993) Modell Simul Mater Sci Eng 1(5):707
27. Kubaschewski O, Goldbeck OV (1949) Trans Faraday Soc 45:948
28. Raghavan V (1992) Indian Inst Metals 6B:1094
29. Syn CK, Jin S, Morris JW (1976) Metall Transac A 7:1827
30. Mun SH, Watanabe M, Li X, Oh KH, Williams DB, Lee HC (2002) Metall Mater Transac A 33:1057
31. Askil J (1970) Tracer diffusion data for metals, alloys and simple oxides. Plenum Publishing Corporation, NY